Article

Coil-to-Bridge Transitions of Self-Assembled Water Chains Observed in a Nanoscopic Meniscus

Byung I. Kim,* Ryan D. Boehm, and Harrison Agrusa

Read Online

ACCESS | Metrics & More | Article Recommendations | Supporting Information

ABSTRACT: Ten downward portions in the large oscillatory force—distance curve reported earlier are analyzed to understand a nanoscale water meniscus confined between a sharp probe and a flat substrate in air. The sigmoidal shape of each portion leads to the assumption that the meniscus is made up of n independent transitions of two states: one for a coil state and the other for a bridge state. The analysis reveals that each downward portion occurs due to a coil-to-bridge transition of n self-assembled water chains whose length ranges between 197 and 383 chain units. The transition provides novel insights into water's unique properties like high surface tension and the long-range condensation distances.
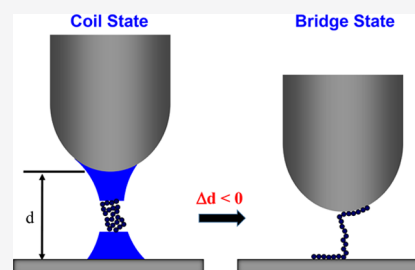
INTRODUCTION

Structures and behaviors of water confined between two surfaces in ambient environments are important in water-based nanoscience and technology such as adhesion,[1] nanolubrication,[2] nanofluidic devices,[3] wetting,[4,5] granular interactions,[6] nanotribology,[7−9] nanolithography,[10] and manipulations of biomolecules using hydration layers.[11] The confined water structures are also critical to various biological processes within a wide range of biological systems.[12] These processes include the formation of micelles and biological membranes,[13] protein folding and assembly,[14] biological recognitions,[15] and ion channelings.[16]

These interactions and processes strongly rely on water's unique properties.[17] Among many of water's unique properties, water's surface tension of 72 mN/m is extremely important. It has been recognized to be the key to the interactions and processes in nature, especially within biological systems (e.g., protein stability in the Hofmeister series[18]). Water's surface tension is known to be the highest among liquids whose molecular dimensions are similar to that of water. Although the high surface tension occurs due to the strong hydrogen bonds among water molecules, the details of this process are not yet well-established.

The latest advancement of force-feedback techniques enables one to measure the meniscus force as a function of the probe—sample distance without the "snap-to-contact" problem associated with atomic force microscopy (AFM) measurement.[19−22] A decade ago, we reported that there are large oscillatory forces, generated by water menisci, as the distance decreases.[23,24] We measured the force—distance curves using a force-feedback technique called the "cantilever-based optical interfacial force microscope" (COIFM) (more experimental details can be found in our earlier publications[23,24]). In the force—distance plot, each oscillation

is composed of a rising-shaped (\) curve in the upward portion and a sigmoidal-shaped (∫) curve in the downward portion as the tip—sample distance decreases (see Figure 1).[24] Further analysis of each upward portion with the freely joined chain (FJC) model reveals that each portion is developed from self-assembled water chains with lengths ranging from 14 to 42 chain units in the meniscus.[24] The chain unit is chosen as the
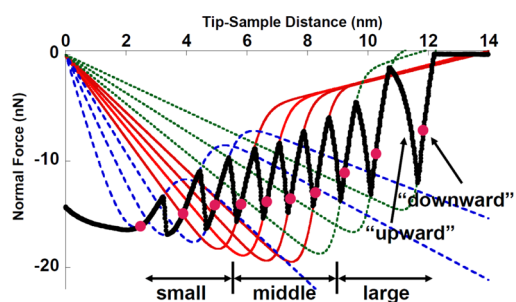

Figure 1. Normal force measured as a function of the separation distance between a probe and a substrate at a relative humidity of 30% and with a probe-approaching speed of 3 nm/s. The dashed line, solid line, and dotted line represent the fitting curves using a two-state transition from a liquid state to a chain state for three different transition distance (d_t) regions. Solid circles represent transition points for each portion. Each d_t is determined by solving the transition condition of two free energies, $g_{liquid}(d_t) = g_{chain}(d_t)$. (Reproduced with permission from ref 24. Copyright 2013 AIP Publishing.)

size of water (σ), which corresponds to 0.275 nm. This choice is supported by the hydrogen bond strength (consistent with the literature value) extracted from the decay length (λ) of 12.86 determined by the analyses of the upward portions.

The downward portions, however, have never been analyzed before even though they take up almost half of each oscillation. In this paper, we analyze each downward portion using two-state Boltzmann statistics. The analysis reveals that each portion is generated by a "coil-to-bridge" transition of self-assembled water chains, whose lengths are between 197 and 383 chain units. This transition provides a new insight into the origin of water's high surface tension and long condensation distances.

MATERIALS AND METHODS

Each downward portion in Figure 1 appears to be a straight line that can be described with two parameters, the slope and the force intercept. The appearance leads to the assumption that the downward portions originate from liquid confined between a flat substrate and a
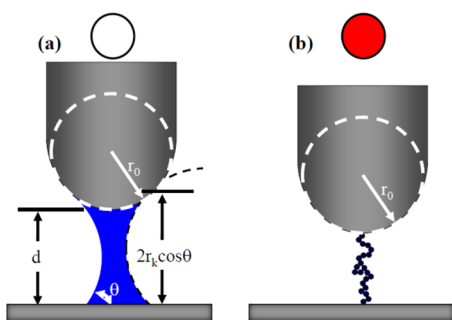
Figure 2. Liquid bridge (a) and chain bridge (b), confined between a flat substrate and a spherical probe with the radius r_0 in air. The open circle represents the former state, and the closed red one represents the latter one.

spherical probe in air (Figure 2a). The confined liquid is known to follow the following AFM force−distance equation:[25,26]

$$f_{liquid}(d) = -4\pi r_0 \gamma \cos\theta \left(1 - \frac{d}{2r_k \cos\theta}\right) \quad (1)$$

where r_k is known as the Kelvin radius, γ is the surface tension of water of 72 mN/m, r_0 is the radius of a spherical probe, d is the probe−substrate distance, and θ is the contact angle. The force becomes zero when the distance d is equal to $2r_k \cos\theta$, which corresponds to the condensation distance for the liquid. Meanwhile, the force response of a single chain confined between a flat substrate and a spherical probe is completely different in Figure 2b. The chain force is well-known to follow the Langevin function, which is successful in describing the rising-shaped (⌡) pattern of upward portions,[24] which is given by[27]

$$d = -l_0 \cdot \sigma \cdot \left[\coth\left(\frac{f_{chain}\sigma}{k_B T}\right) - \left(\frac{k_B T}{f_{chain}\sigma}\right) \right] \quad (2)$$

where f_{chain} is the force by a single chain between the probe and the sample, l_0 is the chain length, k_B is the Boltzmann constant, T is temperature, and σ is the size of the water molecule. When the linear model (eq 1) is applied to the downward portion of the distance range between 3.2 and 4.5 nm in Figure 3a, it can be said to still be a good approximation to the first order with a correlation coefficient (R) of 0.985. However, it is not sufficient to describe the sigmoidal pattern.
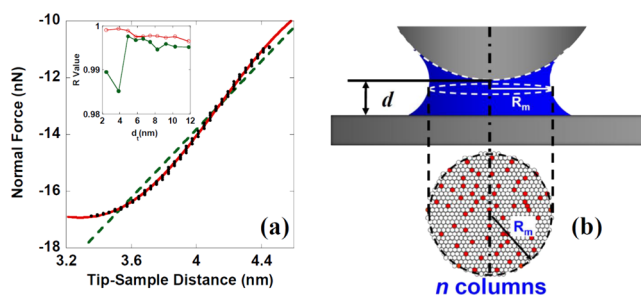
Figure 3. (a) Comparison of fitting methods between linear fitting (green dashed line) and the two-state fitting model (red solid line). (Inset) R value vs the transition distance (d_t) for the two-state fitting (open red circles) and linear fitting (closed green circles). (b) n columns, each of which can be either the liquid state (open circle) or chain one (closed circle) in the water meniscus. R_m represents the radius of the meniscus waist.

In this analysis, the sigmoidal force is viewed as the combination of the liquid force (eq 1) and the chain force (eq 2) according to Boltzmann statistics, as commonly seen in many two-state biophysical systems.[27] The water meniscus is assumed to be made of n columns, each of which takes one of the two states, forming a mixture of n independent states. In Figure 3b, since the radius of the meniscus waist (R_m) is reported to range between 70 and 280 nm at RH = 40−50%,[28] we expect the column number (n) to be thousands assuming that r_0 is ~10σ. Each population is determined by the respective free energies through Boltzmann distribution. The radius r_0 in Figure 2a is now redefined as the radius of a unit spherical probe at a lattice site in Figure 3b. The average force $\langle F(d) \rangle$ of two forces, one from the liquid column and the other from the chain one, over the n columns is given as follows:[29]

$$\langle F(d) \rangle = n \left[\frac{f_{liquid} e^{-g_{liquid}/k_B T} + f_{chain} e^{-g_{chain}/k_B T}}{e^{-g_{liquid}/k_B T} + e^{-g_{chain}/k_B T}} \right] \quad (3)$$

where g_{liquid} and g_{chain} are equilibrium free energies of liquid and chain states, respectively, and $k_B T$ is the thermal energy. At room temperature T_r corresponding to about 298 K, the quantity $k_B T_r$ ($\approx$ 4.1 pN nm) is used as the energy unit in this paper.

We use the average force to fit each of the 10 downward portions embedded in the force−distance plot (Figure 1). It is straightforward to write the liquid force (f_{liquid}) as $f_{liquid}(d) = k_{liquid} \cdot d - f_{l0}$ where k_{liquid} and f_{l0} are a slope and a force intercept, respectively, from eq 1. However, it is challenging to find the chain force f_{chain} as a function of the distance d because the distance d is expressed as a funtion of f_{chain} in the original FJC equation (eq 2). The chain force−distance equation (eq 2) is approximated as $f_{chain} = -\frac{\frac{k_B T}{\sigma}}{1 - \frac{d}{l_0 \sigma}}$ in the high force regime ($f_{chain} >> \frac{k_B T}{\sigma}$ (= 15pN)) where $\coth\left(\frac{f_{chain}\sigma}{k_B T}\right) \approx 1$. While the approximation, named as the "FJC force", is excellent in describing the upward portions, its use as one of the two states in the transition model (eq 3) is unable to reproduce any downward portions. With each sigmoidal shape being relatively monotonous, the steep, concave-down behavior of the force (at the distance d becomes close to $l_0\sigma$) appears to cause the problem. In the low force regime ($f_{chain} << \frac{k_B T}{\sigma}$ where $\coth\left(\frac{f_{chain}\sigma}{k_B T}\right) \approx \frac{k_B T}{f_{chain}\sigma} + \frac{f_{chain}\sigma}{3k_B T} + ...$), eq 2 is approximated as follows:

$$f_{chain} = -k_{chain} d \quad (4)$$

where the spring constant k_{chain} is given by $k_{chain} = \frac{3k_B T}{l_0 \sigma^2}$ for a water chain with the chain length l_0 and the individual monomer size σ.[13] When it is used as one of the two states, the transition model is able to

Table 1. Fitting Results of Each Downward Portion in the Force−Distance Data (Figure 1) Using Equation 3

distance regions	d_t (nm)	k_{chain} (pN/nm)	k_{liquid} (pN/nm)	f_{l0} (pN)	Δg_0 ($k_B T_r$)	n	R
small	2.47	3.73	−0.959	0	−2.07	2778	0.999
	3.88	3.26	−0.798	0	−4.52	1894	0.999
	4.94	3.17	−0.755	0	−7.18	1455	0.999
middle	5.80	2.84	0.504	6.79	−4.11	1380	0.998
	6.65	2.65	0.571	7.57	−5.13	1288	0.998
	7.44	2.52	0.574	7.82	−6.71	1212	0.998
	8.27	2.41	0.596	8.07	−8.75	1124	0.998
large	9.23	2.33	0.598	7.76	−13.0	930	0.997
	10.3	2.08	0.800	8.40	−16.0	862	0.998
	11.8	1.93	0.894	8.31	−24.1	690	0.996

reproduce the downward portion faithfully in Figure 3a. The observation is supported by an R value of 0.999, a dramatic increase from that of 0.985 in the straight line fitting. For the curve fitting, the free energies of both forces are written as $g_{liquid} = -\frac{1}{2}k_{liquid}d^2 + f_{l0}d + g_{l0}$ and $g_{chain} = \frac{1}{2}k_{chain}d^2 + g_{c0}$ with distance-independent free energies, g_{l0} and g_{c0}. The key outcome of this analysis is that the five parameters k_{liquid}, f_{l0}, k_{chain}, n, and Δg_0 (= $g_{c0} - g_{l0}$) are uniquely determined by fitting each downward portion.

■ RESULTS AND DISCUSSION

The two-state transition model is confirmed to be more precise than the linear one when the two-state curve fitting is repeatedly applied to all remaining downward portions in Figure 1. Each fitting curve (the solid lines) faithfully follows its corresponding sigmoidal shape (open circles), showing that the two-state model is excellent in describing the downward portions. The corresponding five fitting parameters and R values are listed for each downward portion in Table 1. The R values are always higher than those of the linear model, as shown in the inset of Figure 3a, thus validating that the two-state model is better than the linear one.

Locating the transition distance (d_t) within a downward interval is important to identify which one is more prevalent between the two states. In Figure 1, solid circles represent the transition points (d_t and $\langle F(d_t)\rangle$) in the downward portions. Each transition distance d_t, listed in Table 1, is determined by solving the transition condition, $g_{liquid}(d_t) = g_{chain}(d_t)$, with the determined k_{liquid}, f_{l0}, k_{chain}, and Δg_0. Since d_t is uniquely determined for each downward portion, it will be used to refer to its corresponding downward portion below. At the distance, the average force $\langle F(d_t)\rangle$ in eq 3 becomes $n\frac{f_{chain}+f_{liquid}}{2}$. The circle is located closer to the left end of its respective downward portion (see Figure 1). In other words, the interval for the liquid bridge ($d > d_t$) takes more portion out of the total downward interval than that of the chain bridge, indicating that the liquid bridge is the prevailing phase in the downward portion. The result explains why the linear model, eq 1, associated with the liquid bridge, is a good approximation in each of downward portions.

The validity of the liquid-to-chain hypothesis is examined by comparing the results in Table 1 with both linear model equations, eqs 1 and 4, for the liquid and chain bridges. For the chain state, k_{chain} decreases from 3.73 to 1.93 pN/nm monotonously as d_t increases in Table 1. The k_{chain} decrease corresponds to the increase in the bridge length, l_0, from 44 to 84 chain units in the chain column state, as l_0 is inversely related to k_{chain} according to the model equation (eq 4). Each fitting curve becomes a line with a negative slope when it is

extrapolated from the transition region to the origin of the force−distance plot (Figure 1). The line is consistent with the model equation, thus confirming that the chain column is one of two states.

The behavior of the liquid state, however, is quite different from the expectation from the model equation (eq 1). While the equation predicts the slope k_{liquid} to be a constant, it increases from −0.959 to +0.894 pN/nm as d_t increases from 2.47 to 11.8 nm in Table 1. The discrepancy is even clearly seen in Figure 1. Seven fitting curves show that they are indeed from liquid columns because they become lines with positive slopes when extrapolated to the region where the distance is larger than d_t (see solid and dotted curves in Figure 1). These seven are consistent with "liquid-to-chain" transitions. On the contrary, for the three remaining transitions where d_t is close to the zero distance (three solid circles in the small d_t region), the extrapolated lines (dashed) have negative slopes despite stemming from liquid columns. We name these three as "chain-to-chain" transitions because both extrapolated lines share the same sign in the slope for each transition portion. Therefore, three chain-to-chain transitions make up the small d_t region, while seven liquid-to-chain transitions make up the middle and large d_t regions.

Furthermore, the liquid force (eq 1) predicts f_{l0} to be directly proportional to k_{liquid} with the proportional constant $2r_k\cos\theta$. However, when the f_{l0} is plotted as a function of k_{liquid} in Figure 3a, it increases linearly only in the middle region while it saturates with zero and 8.16 pN in the small and large regions, respectively. The disagreement in the slope and the intercept between the predicted and analyzed values disproves the initial query about the model (eq 1) that denotes the liquid columns consisting of pure liquid phase water. Based on different behaviors of the f_{l0} depending on the location of d_t (solid circles), we categorize the coil-to-bridge transitions into three groups: "small", "middle", and "large" (see Figure 1).

To resolve the disagreement, we introduce a chain coil with the length L in the liquid column, forming a "two-phase water" as in the model diagram in Figure 5a. The introduction is based on the opposite trends of k_{chain} and k_{liquid} in relation to the distance, which leads to a double-reciprocal plot. Figure 4b shows two lines with slightly different slopes (m's), 4.08 and 4.53, in small and middle d_t regions, respectively. The slope m's value is greater than one, suggesting that the liquid column should have a chain structure whose chain length is m times longer than the bridge length, l_0. The observed strong correlation between k_{chain} and k_{liquid} leads to the assumption that the liquid bridge might be a composite structure that has a chain. The chain introduction modifies the force (eq 1) into

$$f_{liquid}(z_0) = -4\pi r_0 \gamma \cos\theta\left(1 - \frac{d-z_0}{2r_k\cos\theta}\right)$$ where z_0 represents
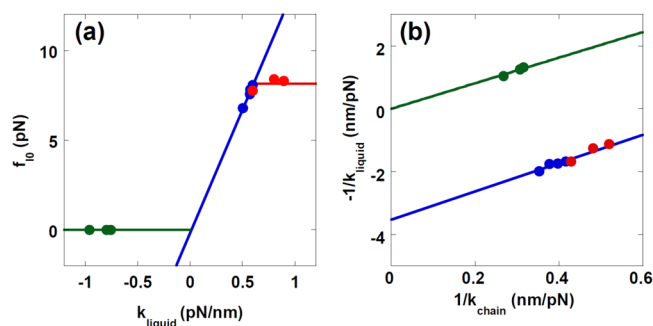
Figure 4. (a) Plot of the force intercept magnitude, f_{l0}, as a function of the slope, k_{liquid}. Data fitting lines are shown for small, middle, and large d_t regions. (b) Double reciprocal plot of $-k_{liquid}$ and k_{chain}. One fitting line is for the small d_t region and the other for the middle and large d_t regions.

the equilibrium length of the coil stretched by the liquid force $f_{liquid}(z_0)$ at a fixed distance d between the two surfaces. Since the coil spring constant k_{coil} is expressed as $k_{coil} = \frac{3k_BT}{L\sigma^2}$, the equilibrium condition is given by $f_{liquid}(z_0) = -k_{coil}z_0$. In the absence of the liquid force (i.e., $f_{liquid}(z_0) = 0$), the length z_0 becomes zero, thus representing the form of a random coil. Eliminating z_0 using the equilibrium condition leads to

$$f_{liquid}(d) = -4\pi r_0 \gamma \cos \theta \left(\frac{2r_k \cos \theta - d}{2r_k \cos \theta - d_0} \right) \text{ where } d_0 = \frac{4\pi r_0 \gamma \cos \theta}{k_{coil}}.$$

The distance d_0 represents the distance where both ends of a coil start to contact both surfaces. It is dependent on the chain length L because the coil spring constant is proportional to the total length L. When the distance d is less than the contact distance d_0, the liquid force simply becomes a chain force $f_{liquid}(d) = -k_{coil}d$ since both chain ends are tethered to their respective surfaces. Therefore, the force is divided into two regions, depending on where the probe–sample distance d is with respect to d_0. The liquid force $f_{liquid}(d)$ is renamed as the "coil force" $f_{coil}(d)$ to emphasize the coil configuration in Figure 5a. Then, the coil force is rewritten as follows:

$$f_{coil}(d) = \begin{cases} -k_{coil}d & \text{for } d < d_0 \\ -4\pi r_0 \gamma \cos \theta \left(\frac{2r_k \cos \theta - d}{2r_k \cos \theta - d_0} \right) & \text{for } d \geq d_0 \end{cases}$$
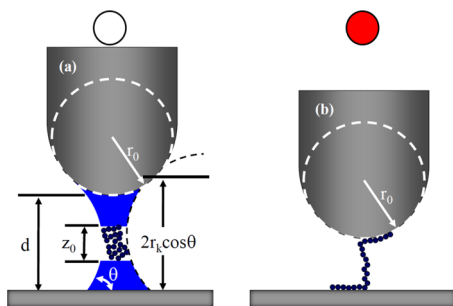
(5)

Figure 5. Model diagrams that represent (a) coil and (b) bridge states, where r_0 is the radius of a unit spherical probe at a lattice site, d is the probe–substrate distance, r_k is the Kelvin radius, and θ is the contact angle. In the coil state, the coil is stretched to the distance length of z_0 between the two surfaces at a fixed distance d. The open circle represents the coil state, while the closed red one represents the bridge state.

The force–distance equation predicts the same condensation distance $2r_k \cos \theta$ (at which the liquid force becomes zero) to be independent of d_0 or the chain length. This means that all chains are already in the liquid bridge (coil state) once the distance is less than $2r_k \cos \theta$.

The observation that $1/k_{coil}$ is equal to m/k_{chain} in the small d_t region (green circles in Figure 4b) leads to the relation that $k_{chain} = mk_{coil}$. Similar to the liquid force, the chain force (f_{chain}) is now renamed with the "bridge force" f_{bridge} as

$$f_{bridge}(d) = -mk_{coil}d \tag{6}$$

Because the chain length is inversely related to the spring constant, m becomes the ratio between the two chain lengths during the transition or L/l_0. The only chain portion that contributes to the measured force is the middle segment between the two surfaces (not on the surfaces). Since $k_{liquid} = \frac{4\pi r_0 \gamma \cos \theta}{2r_k \cos \theta - d_0}$ from eq 5, its reciprocal presents

$$\frac{1}{k_{liquid}} + \frac{m}{k_{chain}} = \frac{2r_k \cos \theta}{4\pi r_0 \gamma \cos \theta} \tag{7}$$

The equation reproduces the double-reciprocal relationship observed in Figure 4b. Because m's are found to be 4.08 and 4.53 from Figure 4b's slopes, roughly 25 (= 1/4.08) and 22% (1/4.53) of chain units in a coil become a bridge in the small and middle regions, respectively. The ratios are used to determine the coil length L. Table 2 shows that L ranges from

Table 2. The Distance of a Coil-to-Bridge Transition (d_t), the Total Number of Liquid and Chain Columns (n), the Chain Length in the Stem after the Transition (l_0), m (= L/l_0), the Coil Chain Length (L), the Radius of Gyration (R_g), the Number of Accumulated Columns (n_a), and the Radius of the Meniscus Waist (R_m)

d_t (nm)	n	l_0 (chain units)	m (= L/l_0)	L (chain units)	R_g (nm)	n_a	R_m (nm)
2.47	2778	44	4.08	197	1.58	13,613	193
3.88	1894	50		226	1.69	10,835	185
4.94	1455	51		232	1.71	8941	170
5.80	1380	57	4.53	260	1.81	7486	164
6.65	1288	61		278	1.87	6106	153
7.44	1212	65		292	1.92	4818	140
8.27	1124	68		306	1.96	3606	124
9.23	930	70	4.53	316	1.99	2482	104
10.3	862	78		355	2.11	1552	87.4
11.8	690	84		383	2.20	690	60.6

197 to 383 chain units in the liquid column for the change of l_0 from 44 to 84. Since the chain length of l_0 across the gap is $1/m$ fraction of L, the "bridge state" is modeled as the configuration of the same chain coil whose l_0/L portion bridges between the two surfaces, as shown in Figure 5b. The bridge state consists of two microphases: the middle segment with the length l_0 and the remaining segments with the length $L - l_0$ adsorbed on both surfaces.

Furthermore, the coil force (eq 5) predicts that, when the distance d is larger than d_0, the force intercept f_{l0} is directly related to the slope k_{liquid} through the condensation distance $2r_k \cos \theta$, as follows: $f_{l0} = 2r_k \cos \theta \cdot k_{liquid}$. The relationship allows us to determine the condensation distance to be 13.5 nm from the slope of the linear portion in Figure 4a. The

vertical intercept in eq 7 represents the ratio between the condensation distance ($2r_k \cos \theta$) and the magnitude of the adhesion force ($-4\pi r_0 \gamma \cos \theta$). The intercept, 3.53 nm/pN, in the middle region allows the adhesion force ($-4\pi r_0 \gamma \cos \theta$) to be determined with -3.81 pN from the condensation distance ($2r_k \cos \theta$) of 13.5 nm (from the slope in Figure 4a). Then, the contact distance d_0 follows $0.0225\ L$ in nm at room temperature because $d_0 = \frac{4\pi r_0 \gamma \cos \theta}{k_{coil}}$. These results suggest that the "coil-to-bridge" transition of the two-phase water (Figure 5a) provides a unified view of the liquid-to-chain and the chain-to-chain transitions observed in Figure 1. The liquid-to-chain transition occurs when $d > d_0$, whereas the chain-to-chain one does when $d < d_0$ in eq 5.

The origin of coils is investigated by plotting the chain number (n) as a function of the coil length L (Figure 6). The
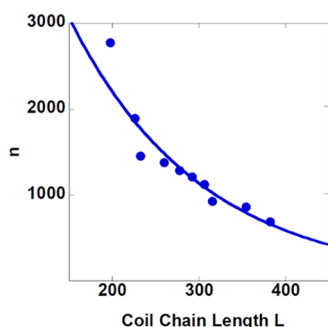

Figure 6. Plot of coil numbers n as a function of the coil length L. (Solid line) Fitting curve with the exponential function $n = n_0 \exp(-L/\lambda_{coil})$ where the decay length (λ_{coil}) and the prefactor (n_0) are determined to be 126 chain units and 11,800 chains, respectively.

size distribution shows that, as L increases from 197 to 383, n decays exponentially from 2780 to 690 following $n = n_0 \exp(-L/\lambda_{coil})$ where n_0 is a prefactor. A similar behavior has been previously observed in the FJC chains self-assembled in chemical equilibrium with vapor.[24] The decay length (λ_{coil}) is 126 chain units (Figure 6), which is longer by an order of magnitude than 12.86 chain units in vapor. Assuming that the concentration $C = 1$ for liquid water, the intermolecular bond strength, $\alpha k_B T_r$, is calculated to be 9.67 $k_B T_r$ from $\lambda_{coil} = \sqrt{Ce^\alpha}$ according to self-assembly theory.[30] The result is in excellent agreement with the hydrogen bonding strength of 10 $k_B T_r$ in the literature (e.g., ref 31), thus confirming that the observed chains arise from self-assembly in equilibrium with the liquid phase. While each chain length L is conserved on average for each downward curve due to its equilibrium with liquid monomers, the amount of liquid changes with the distance to maintain the Kelvin radius r_k in equilibrium. Therefore, the total mass of the two-phase water changes with the distance.

The force generated during the coil-to-bridge transition provides a novel insight into the surface tension. Water is known to have a much greater surface tension than other liquids with nonpolar molecules of similar sizes.[26] The maximum coil force $-4\pi r_0 \gamma \cos \theta$ increases to the bridge force, $m \times (-4\pi r_0 \gamma \cos \theta)$ at $d = d_0$ in eq 6. Since m is either 4.08 or 4.53, the coil-to-bridge transition dramatically increases force roughly by a factor of 4. Without the transition, water's surface tension of 72 mN/m would become 18 mN/m,

matching the surface tensions of small nonpolar molecules like n-pentane (15.5 mN/m) and n-hexane (17.9 mN/m).[26]

It is important to estimate the radius of the meniscus waist (R_m) with information available in Table 2 since it can be compared with the R_m values directly measured by scanning electron microscopy (SEM).[28] Assuming that the coils are highly packed in the middle of the meniscus, the sectional area (A) can be written as $A = n_a \times 2\sqrt{3} R_g^2$ where n_a is the accumulated number of chains and R_g is the radius of gyration, related to the chain length L as $R_g = \frac{\sigma \sqrt{L}}{\sqrt{6}}$.[30] The calculated R_m from $\sqrt{\frac{A}{\pi}}$ ranges between 60 and 190 nm (in Table 2), which is surprisingly close to the reported range between 70 and 280 nm at RH = 40–50%.[28] The result confirms the validity of our approach to use Boltzmann statistics to analyze the force–distance curve.

The next question is how a self-assembled long chain forms the coil structure, which extends up to the long condensation distance $2r_k \cos \theta$ of 13.5 nm in Figure 4a, considering that the capillary condensation theory predicts the length scale of a stable meniscus to be less than 1 nm or so at an RH of 30%. Recently, Kim et al. explained the systematic difference between the observed condensation distance and the one predicted by the Kelvin equation using the curvature-dependent surface tension of a meniscus at a molecular scale.[32] However, the correction distance or Tolman's length is analyzed to be just ~0.2 nm, indicating that the theory needs to be revised to fully describe experimental observations. Formation of a long-range meniscus through the elongation and subsequent merges of an additional surface water layer is unlikely because the liquid meniscus should follow the Kelvin equation with the slow tip speed of 3 nm/s. Instead of vapor condensation in the Kelvin theory, the observed long-range condensation distance is accounted for by the condensation of the FJC chains, identified in the earlier analysis of upward portions.[24] The chemical potential difference between the FJC chain phase and liquid is significantly smaller than that between vapor and liquid. According to self-assembly theory,[13,30] the chemical potential is given by $\mu_{short\ chain}(C) = -\left(\alpha + \frac{1}{\sqrt{C}e^\alpha}\right)k_B T_r$ where $\alpha k_B T_r$ is the hydrogen bond strength and C is the humidity in mole fraction. The chemical potential difference, $\mu_{short\ chain} - \mu_{liquid}$, between FJC chains at an RH of 30% ($C = 7.75 \times 10^{-3}$) and liquid ($C = 1$) is just $-6.98 \times 10^{-2}\ k_B T_r$, which is 17 times smaller than that between vapor and liquid. The Kelvin radius is defined as the ratio between the surface tension and the chemical potential difference (i.e., $r_k = \gamma/\Delta\mu$), which leads to a new Kelvin radius r_k as follows:

$$r_k(C) = \frac{\gamma v_m}{k_B T} \frac{\sqrt{e^\alpha}}{\left(1 - \frac{1}{\sqrt{C}}\right)} \tag{8}$$

The stable bridge's formation distance $2r_k$ is predicted to be 14.9 nm. When the contact angle θ is chosen with 30° for the reported range between 17 and 42° on oxidized silicon substrates,[23] the value of $2r_k \cos \theta$ is calculated to be 12.9 nm, matching the observed condensation distance of 13.5 nm.

The effect of probe curvature on the oscillatory force is investigated by measuring the force–distance curves with a hydrophilic silica probe with the tip radius of ~100 nm,
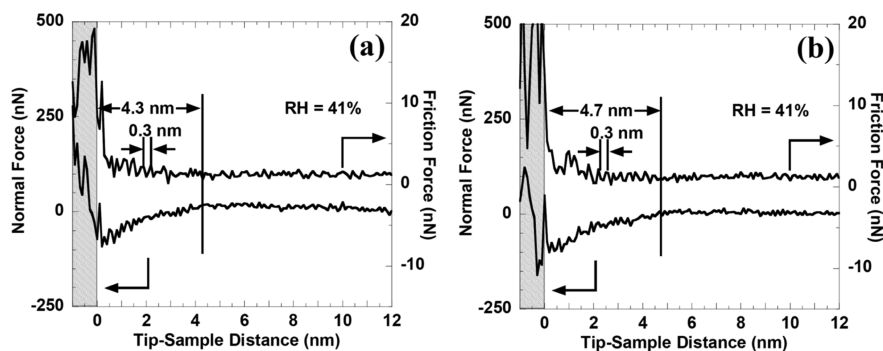
Figure 7. Normal and friction force profiles as a function of the separation distance (a) on approach and (b) on retraction between an optical-fiber tip and a silicon surface taken at an RH of 41%. The periodicity is ~0.3 nm, the dimension of a single water molecule.

roughly 10 times larger than the typical AFM probe size. The measurements are performed with the same probe speed of 0.1 nm/s during the probe approaching toward and retraction from the surface at the relative humidity of 41% by interfacial force microscopy (IFM). Interestingly, the approaching curve (Figure 7a) shows that any appreciable forces in both friction and normal force channels appear at the distance of 4.3 nm. The shorter onset distance is roughly one-third of the condensation distance $2r_k \cos\theta$. While the friction force shows oscillatory peaks with the periodicity of the water molecular size of ~0.3 nm, the normal force curve presents an almost linear pattern without presenting any noticeable oscillatory feature. The force behavior is almost reproducible in the retraction curve (Figure 7b), showing the reversibility of the force curve. The oscillation in the friction force is attributed to the well-known high signal selectivity of the lock-in technique in comparison to the DC measurement (i.e., the normal force) in the noisy electrical signal.[33] The oscillatory feature in friction is again interpreted as the combined effect of the coil-to-bridge transitions of the two-phase water (downward portion) and the FJC forces (upward portion).

The reversibility is understood with two different types of unusual long nucleation times (up to the order of seconds), recently reported in the nanoscopic menisci.[9,34−37] We associate the nucleation time larger than ~300 ms[9,34−36] with the coil-to-bridge transition, whereas the shorter time (~3 ms)[34,37] with a two-state transition, named the "brush-to-FJC transition" for the formation of the FJC bridge.[38] This association is based on the known scaling relation $1/\tau = 1/(L^2\zeta)$ where τ is a nucleation time, L is the chain length and ζ is the friction coefficient per segment.[39] The relation predicts that the FJC chains are found to be roughly a hundred times faster than the long chains. At the speed of 0.1 nm/s, the coil-to-bridge transition is an equilibrium process because both nucleation times are much smaller than the tip dwelling time. It takes 3 s for the tip to travel the smallest transition length scale (the size of the water molecule σ or 0.3 nm), meaning that the forward and backward transitions are equally probable. In equilibrium, the oscillation transition is dictated by the FJC chain length that matches the probe−sample spacing, rather than the nucleation times. This explains why we observe the periodicity of ~0.3 nm in Figure 7a,b. This equilibrium condition does not hold when the tip speed is higher than σ/τ (~1 nm/s), which corresponds to the threshold speed. The process becomes a kinetically activated one when the speed is higher than the threshold speed of ~1 nm/s. In this speed regime, the number of oscillations and the transition positions

are different between the approaching and retraction curves, as seen in the data reported earlier.[40]

The observed shorter onset distance of ~4 nm is the averaging effect of the larger probe on the force. The absence of the oscillatory feature in normal channels suggests that the nanoscale surface roughness of the larger probe results in an interference effect among FJC chain forces through the d variation in eq 2. The effect leads to the averaging of the FJC chain length (l) over the distribution of the number of chains (n_l), which is given by $n_l = n_0 \exp\left(-\frac{l}{\lambda}\right)$ where n_0 and λ represent the prefactor and the decay length, respectively.[24] The average chain length $\langle l \rangle$ is given by λ as follows:

$$\langle l \rangle = \frac{\sum_{l=0}^{\infty} l \cdot n_l}{\sum_{l=0}^{\infty} n_l} = \lambda \tag{9}$$

Since the decay length λ is ~13 and the chain unit (σ) is the molecular size of water (~0.3 nm), the average distance $\langle l\sigma \rangle$ is ~4 nm, accounting for the observed onset distances in Figure 7a and the IFM data reported by Houston and his colleagues.[41,42] The analysis confirms that the water chain model is valid in describing the onset distance even for a larger meniscus confined between two hydrophilic surfaces.

The effect of surface wettability on the force curves is studied by collecting the IFM force−distance curves on the same oxidized silicon surface but with a hydrophobic IFM probe. The force patterns are similar to those taken by the hydrophilic probe although the force magnitude is weaker (Figure 8). The onset distance is even shorter with 2.8 nm, roughly 70% of that taken with the hydrophilic probe. The coil-to-bridge transition is driven by chain adsorption, theoretically predicted by earlier adsorption studies of a single polymer chain, tethered to an AFM probe on a surface.[43] The adsorption energy is decreased by a factor of two since the hydrophobic probe can be considered to be inert. The onset distance is predicted to depend on the square root of the adsorption energy (see the Supporting Information), which leads to $\sim\frac{1}{\sqrt{2}}$, thus explaining why we observe 70% of that taken between two hydrophilic surfaces. Therefore, the effect of the wettability on the onset distance is accountable within the frame of the coil-to-bridge transition model, although additional analysis in conjunction with the fifth parameter Δg_0 would provide more quantitative prediction.

So far, we have successfully identified the coil-to-bridge transition of self-assembled long water chains using five adjustable parameters (k_{liquid}, f_{l0}, k_{chain}, n, and Δg_0). In contrast,
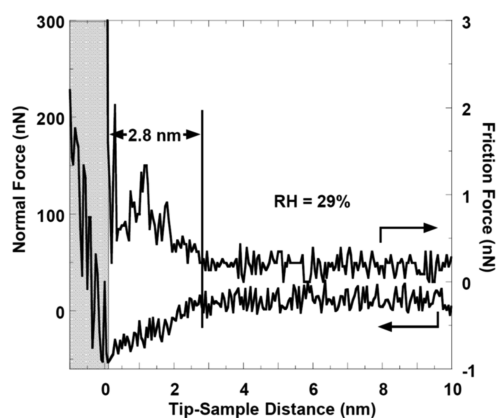
Figure 8. Normal force and friction force profiles versus the tip-to-sample distance between a fluorocarbon-coated silica tip and a silicon surface taken on approach at a 29% RH. Several peaks in friction and an attraction peak in the normal force are shown in the distance range between 0 and 2.8 nm.

the fitting to the upward portions using the FJC force, reported earlier, has only two parameters (the total number of chains n and the chain length l) to fit the upward portions.[24] The n FJC chains form a bundle that bridges the probe and the sample surface through the brush-to-FJC transition.[38] A brush structure should be introduced to account for the activation barrier of ~20 $k_B T_r$ reported earlier[34] because the activation energy from a random coil to the FJC chain is estimated to be ~60 $k_B T_r$.[38] The van der Waals (vdW) interactions among the elongated chains appear to be the origin of brush formation. Although the vdW pairwise interaction is weaker than that of a hydrogen bond by an order of magnitude,[13] the total sum of all interactions along the stretched chains should be strong enough to put them together since the length ranges between 14 and 42. During the bridge formation, the chains with the same length are selected to gather together and form an FJC bridge between both the tip and sample surfaces. The bridge formation creates an additional energy as the hydrogen bonds between the chains and both the tip and sample surfaces. Therefore, the chain length should be conserved for a given bridge. Interestingly, each chain in the bridge still follows the FJC force,[24] rather than a spring-like force that represents a three-dimensional bulk network (e.g., a hydrogel).

This vertically aligned brush structure on the silicon surface exists only when the relative humidity is less than 40%. Otherwise, the oscillatory pattern becomes drastically weaker.[23] This observation is supported by earlier humidity-dependent AFM studies, which have reported the growth of "liquid-like" water once the relative humidity becomes higher than ~50%.[1,44−46] The drastic pattern weakness is also observed on the silicon surface, which is covered with a thick layered structure.[47] The layered structure appears to promote the lateral growth of the water film rather than the vertical growth from the FJC chains.

The kinetically activated process of the coil-to-bridge transition in conjunction with the brush-to-FJC transition offers an explanation as to why a sharp transition happens between a downward portion and its subsequent upward portion and vice versa. Since ~80% (= $1 − 1/m$) of the chain units make a transition from the coil state to the bridge state, the space under the probe is available to the FJC chains.[24] They quickly take over the space under the probe and form an FJC bridge through the brush-to-FJC transition. As the

distance continues to decrease, the FJC bridge generates the upward portion in the force−distance curve. Meanwhile, the population of long chains grows slowly, which builds up the elastic energy of the FJC bundle by their steric interactions. The FJC bridge is abruptly unbounded from both surfaces at a certain threshold point, which corresponds to the transition from upward to downward portions. In this explanation, the oscillatory force is mainly driven by the coil-to-bridge transition, which is supported by large smooth oscillations observed at water/air interfaces by Teschke and de Souza.[48]

Finally, the finding of the coil-to-bridge transition has huge implications in understanding nanoscopic water. Theoretically, the chain formation can be explained with the MB (Mercedes-Benz) model,[49] one of the most successful water models. In the MB model, each water molecule next to an extended hydrophobic surface loses one hydrogen bond, thus leaving two out of three hydrogen bonds. The two bonds form a chain through a self-assembly process. This mechanism is supported by the disappearance of an attractive force when a hydrophilic probe is immersed in liquid water,[21] indicating that hydrophobic hydration layers are crucial for the attractive force both in liquid water and in air. Other supporting earlier reports include AFM observation of an interconnected water network,[50] a clathrate network made of ~400 water molecules confined in an antifreeze protein,[51] long-range structural ordering of water at water−air interfaces,[48] observation of hydrogen-bonded chains or rings by photoemission spectroscopy,[52] multibranched polymer chains with the length of 150 water monomers observed by novel quantum force field molecular dynamics,[53] and a long water chain structure along DNA grooves.[54] The new knowledge acquired through this study will contribute to the advancements in water-based nano/biosciences and technology such as nanotribology.

■ CONCLUSIONS

We analyze 10 downward portions of the oscillatory force−distance curve data taken from a nanoscopic water meniscus confined between two hydrophilic surfaces in air by the COIFM. Our statistical analysis of the force−distance curve leads to a novel water structure named "two-phase water" made of self-assembled chains and liquid in a meniscus. The self-assembled chains with the length ranging from 197 to 383 chain units (water diameters) experience unique "coil-to-bridge transitions." The transitions account for water's high surface tension of 72 mN/m and the earlier observation of larger radii of menisci observed by scanning electron microscopy. The two-phase water forms from the condensation of other short self-assembled chains (with lengths ranging from 14 to 42 chain units) in equilibrium with vapor. The Kelvin radius based on this condensation explains the observed long-range condensation distances, which are dependent on probe curvature and surface wettability. The difference in the nucleation time between the two self-assembled chains (due to their chain length difference) offers a mechanism of an oscillatory force and its reversibility between two force curves in which one is taken on approach and the other is on retraction.

■ ASSOCIATED CONTENT

ⓢ Supporting Information

The Supporting Information is available free of charge at https://pubs.acs.org/doi/10.1021/acs.langmuir.1c03100.

Dependence of the transition distance on the chemical potential difference and the initiation energy (PDF)

AUTHOR INFORMATION

Corresponding Author

    Byung I. Kim − *Department of Physics, Boise State University, Boise, Idaho 83725, United States;* ⊙ orcid.org/0000-0003-4484-1728; Email: ByungKim@boisestate.edu

Authors

    Ryan D. Boehm − *Department of Physics, Boise State University, Boise, Idaho 83725, United States*

    Harrison Agrusa − *Department of Physics, Boise State University, Boise, Idaho 83725, United States*

Complete contact information is available at:

https://pubs.acs.org/10.1021/acs.langmuir.1c03100

Notes

The authors declare no competing financial interest.
The data that support the findings of this study are available within the article.

REFERENCES

(1) Asay, D. B.; Kim, S. H. Effects of adsorbed water layer structure on adhesion force of silicon oxide nanoasperity contact in humid ambient. *J. Chem. Phys.* **2006**, *124*, 174712−174715.

(2) Khan, S. H.; Matei, G.; Patil, S.; Hoffmann, P. M. Dynamic solidification in nanoconfined water films. *Phys. Rev. Lett.* **2010**, *105*, 106101−106104.

(3) Squires, T. M.; Quake, S. R. Microfluidics: Fluid physics at the nanoliter scale. *Rev. Mod. Phys.* **2005**, *77*, 977−1026.

(4) Verdaguer, A.; Sacha, G. M.; Bluhm, H.; Salmeron, M. Molecular structure of water at interfaces: Wetting at the nanometer scale. *Chem. Rev.* **2006**, *106*, 1478−1510.

(5) Lee, K.; Kim, Q.; An, S.; An, J. H.; Kim, J.; Kim, B.; Jhe, W. Superwetting of TiO2 by light-induced water-layer growth via delocalized surface electrons. *Proc. Natl. Acad. Sci. U. S. A.* **2014**, *111*, 5784−5789.

(6) Barabasi, A.-L.; Albert, R.; Schiffer, P. The physics of sand castles: maximum angle of stability in wet and dry granular media. *Phys. A* **1999**, *266*, 366−371.

(7) Li, Q.; Tullis, T. E.; Goldsby, D.; Carpick, R. W. Frictional ageing from interfacial bonding and the origins of rate and state friction. *Nature* **2011**, *480*, 233−236.

(8) Barel, I.; Filippov, A. E.; Urbakh, M. Formation and rupture of capillary bridges in atomic scale friction. *J. Chem. Phys.* **2006**, *124*, 174712−174716.

(9) Jinesh, K. B.; Frenken, J. W. M. Capillary Condensation in Atomic Scale Friction: How Water Acts like a Glue. *Phys. Rev. Lett.* **2006**, *96*, 166103−166104.

(10) Hong, S.; Mirkin, C. A. A nanoplotter with both parallel and serial writing capabilities. *Science* **2000**, *288*, 1808−1811.

(11) Huber, D. L.; Maginell, R. P.; Samara, M. A.; Kim, B.-I.; Bunker, B. C. Programmed Adsorption and Release of Proteins in a Microfluidic Device. *Science* **2003**, *301*, 352−354.

(12) Ball, P. Water as an Active Constituent in Cell Biology. *Chem. Rev.* **2008**, *108*, 74−108.

(13) Jones, R. A. L. *Soft Condensed Matter.* New York, USA: Oxford University Press, 2002.

(14) Voet, D.; Voet, J.; Pratt, C. *Fundamentals of Biochemistry 2nd Edition: Life at the Molecular Level*, John Wiley & Sons, New York, 2006, pp. 157.

(15) Castellano, R. K.; Diederich, F.; Meyer, E. A. Interactions with aromatic rings in chemical and biological recognition. *Angew. Chem., Int. Ed.* **2003**, *42*, 1210−1250.

(16) Aryal, P.; Sansom, M. S. P.; Tucker, S. J. Hydrophobic Gating in Ion Channels. *J. Mol. Biol.* **2015**, *427*, 121−130.

(17) Wiggins, P. M. High and low density water in gels. *Prog. Polym. Sci.* **1995**, *20*, 1121−1163.

(18) Moghaddam, S. Z.; Thormann, E. The Hofmeister series: Specific ion effects in aqueous polymer solutions. *J. Colloid Interface Sci.* **2019**, *555*, 615−635.

(19) Bonander, J. R.; Kim, B. I. Cantilever based optical interfacial force microscope. *Appl. Phys. Lett.* **2008**, *92*, 103124−103123.

(20) Kim, B. I.; Bonander, J. R.; Rasmussen, J. A. Simultaneous measurement of normal and frictional forces using a cantilever-based optical interfacial force microscope. *Rev. Sci. Instrum.* **2011**, *82*, 053711−053715.

(21) Kim, B. I.; Smith, L.; Tran, T.; Rossland, S.; Parkinson, E. Cantilever-based optical interfacial force microscope in liquid using an optical-fiber tip. *AIP Advances* **2013**, *3*, 032126−032125.

(22) Goertz, M. P.; Moore, N. W. Mechanics of soft interfaces studied with displacement-controlled scanning force microscopy. *Prog. Surf. Sci.* **2010**, *85*, 347−397.

(23) Kim, B. I.; Rasmussen, J. A.; Kim, E. J. Large oscillatory forces generated by interfacial water under lateral modulation between two hydrophilic surfaces. *Appl. Phys. Lett.* **2011**, *99*, 201902−201903.

(24) Kim, B. I.; Boehm, R. D.; Bonander, J. R. Direct observation of self-assembled chain-like water structures in a nanoscopic water meniscus. *J. Chem. Phys.* **2013**, *139*, 054701−054707.

(25) Barthel, E.; Lin, X. Y.; Loubet, J. L. Adhesion Energy Measurements in the Presence of Adsorbed Liquid Using a Rigid Surface Force Apparatus. *J. Colloid Interface Sci.* **1996**, *177*, 401−406.

(26) Butt, H. J.; Kappl, M. Normal Capillary Forces. *Adv. Colloid Interface Sci.* **2009**, *146*, 48−60.

(27) Phillips, R.; Kondev, J.; Theriot, J. *Physical Biology of the Cell*, Garland Science, New York, (2009).

(28) Weeks, B. L.; Vaughn, M. W.; DeYoreo, J. J. Direct imaging of meniscus formation in atomic force microscopy using environmental scanning electron microscopy. *Langmuir* **2005**, *21*, 8096−8098.

(29) Nelson, P. *Biological Physics*. W.H. Freeman & Co., New York, (2004).

(30) Israelachvili, J. N. *Intermolecular and Surface Forces*, 2nd ed. (Academic Press, Inc., San Diego, CA, (1991).

(31) Marin, A.; Warbrick, J.; Cammarata, A. *Physical Pharmacy* 3rd Ed. Lea & Febiger, Philadelphia (1983)

(32) Kim, S.; Kim, D.; Kim, J.; An, S.; Jhe, W. Direct Evidence for Curvature-Dependent Surface Tension in Capillary Condensation: Kelvin Equation at Molecular Scale. *Phys. Rev. X* **2018**, *8*, 041046−041014.

(33) Meade, M. L. *Lock-in Amplifiers: Principles and Applications.* Peter Peregrinus Ltd. London, UK (1983).

(34) Szoszkiewicz, R.; Riedo, E. Nucleation Time of Nanoscale-Water Bridges. *Phys. Rev. Lett.* **2005**, *95*, 135502−135504.

(35) Greiner, C.; Felts, J. R.; Dai, Z.; King, W. P.; Carpick, R. W. Local Nanoscale Heating Modulates Single-Asperity Friction. *Nano Lett.* **2010**, *10*, 4640−4645.

(36) Sung, B.; Kim, J.; Stambaugh, C.; Chang, S.-J.; Jhe, W. Direct measurement of activation time and nucleation rate in capillary-condensed water nanomeniscus. *Appl. Phys. Lett.* **2013**, *103*, 213107−213104.

(37) Vitorino, M. V.; Vieira, A.; Marques, C. A.; Rodrigues, M. S. Direct measurement of the nucleation time of a water nanobridge. *Sci. Rep.* **2018**, *8*, 13848−13848.

(38) Kim, B. I.; Boehm, R. D. *Brush-to-FJC Transitions of Self-Assembled Water Chains through Capillary Condensation in a Nanoscopic Meniscus, in preparation.*

(39) Klushin, L. I.; Skvortsov, A. M.; Leermakers, F. A. M. Exactly solvable model with stable and metastable states for a polymer chain near an adsorbing surface. *Phys. Rev. E* **2002**, *66*, 036114−036111.

(40) Kim, B. I.; Boehm, R. D. Imaging Stability in Force-Feedback High-Speed Atomic Force Microscopy. *Ultramicroscopy* **2013**, *125*, 29−34.

(41) Major, R. C.; Houston, J. E.; McGrath, M. J.; Siepmann, J. I.; Zhu, X.-Y. Viscous water meniscus under nanoconfinement. *Phys. Rev. Lett.* **2006**, *96*, 177803−177804.

(42) Goertz, M. P.; Houston, J. E.; Zhu, X.-Y. Hydrophilicity and the Viscosity of Interfacial Water. *Langmuir* **2007**, *23*, 5491−5497.

(43) Klushin, L. I.; Skvortsov, A. M.; Polotsky, A. A.; Hsu, H.-P.; Binder, K. Coil-bridge transition in a single polymer chain as an unconventional phase transition: Theory and simulation. *J. Chem. Phys.* **2014**, *140*, 204908−204911.

(44) Sumner, A. L.; Menke, E. J.; Dubowski, Y.; Newberg, J. T.; Penner, R. M.; Hemminger, J. C.; Wingen, L. M.; Brauers, T.; Finlayson-Pitts, B. The nature of water on surfaces of laboratory systems and implications for heterogeneous chemistry in the troposphere. *Phys. Chem. Chem. Phys.* **2004**, *6*, 604−613.

(45) Sedin, D. L.; Rowlen, K. L. Adhesion Forces Measured by Atomic Force Microscopy in Humid Air. *Anal. Chem.* **2000**, *72*, 2183−2189.

(46) Xiao, X. D.; Qian, L. M. Investigation of Humidity-Dependent Capillary Force. *Langmuir* **2000**, *16*, 8153−8158.

(47) Kim, B. I.; Boehm, R. D. Mechanical Property Investigation of Soft Materials by Cantilever-Based Optical Interfacial Force Microscopy. *Scanning* **2013**, *35*, 59−67.

(48) Teschke, O.; de Souza, E. F. Water molecule clusters measured at water/air interfaces using atomic force microscopy. *Phys. Chem. Chem. Phys.* **2005**, *7*, 3856−3865.

(49) Southall, N. T.; Dill, K. A. The Mechanism of Hydrophobic Solvation Depends on Solute Radius. *J. Phys. Chem. B* **2000**, *104*, 1326−1331.

(50) Xu, L.; Lio, A.; Hu, J.; Ogletree, D. F.; Salmeron, M. Wetting and capillary phenomena of water on mica. *J. Phys. Chem. B* **1998**, *102*, 540−548.

(51) Sun, T.; Lin, F. H.; Campbell, R. L.; Allingham, J. S.; Davies, P. L. An Antifreeze Protein Folds with an Interior Network of More than 400 Semi-Clathrate Waters. *Science* **2014**, *343*, 795−798.

(52) Wernet, P.; Nordlund, D.; Bergmann, U.; Cavalleri, M.; Odelius, M.; Ogasawara, H.; Naslund, L. A.; Hirsch, T. K.; Ojamae, L.; Glatzel, P.; Pettersson, L. G. M.; Nilsson, A. The structure of the first coordination shell in liquid water. *Science* **2004**, *304*, 995−999.

(53) Naserifara, S.; Goddard, W. A., III Liquid water is a dynamic polydisperse branched polymer. *Proc. Natl. Acad. Sci. U. S. A.* **2019**, *116*, 1998−2003.

(54) McDermott, M. L.; Vanselous, H.; Corcelli, S. A.; Petersen, P. B. DNA's Chiral Spine of Hydration. *ACS Cent. Sci.* **2017**, *3*, 708−714.